Impact of MODIS BRDF and Albedo on Land Surface Models

Zhuo Wang, Xubin Zeng, Michael Barlage (Department of Atmospheric Sciences, The University of Arizona, Tucson, AZ 85721, zhuowang@atmo.arizona.edu)
Robert Dickinson (Georgia Institute of Technology, Atlanta, GA), Crystal Schaaf, and Feng Gao (Boston University, Boston, MA)

1. Introduction

Land surface albedo describes the fraction of incoming solar energy reflected at a given point and time, and hence determines the surface temperature and evapotranspiration. It is strongly dependent on the solar zenith angle (SZA) and the 3-D structure of vegetation canopy. The land surface albedo in regional and global models can be specified using empirical observations or computed based on a radiation submodel for canopy plus underlying soil. These approaches do not consider the 3-D structure of vegetation.

To improve model treatment of surface albedo, the SZA dependence of albedo in the NCAR Community Climate System Model (CCSM2; Blackmon et al. 2001) as well as model monthly averaged albedo and direct solar beam albedo at local noon are evaluated using the MODIS BRDF data. These studies as well as the MODIS BRDF and albedo data will provide a good starting point towards the development of a BRDF-based treatment of radiative transfer within canopy for regional and global models.

2. Model albedo and MODIS BRDF and albedo data

a. Model albedo

The CCSM2 albedo is computed in its land surface component, that is, the Community Land Model (CLM2; Bonan et al. 2002). The albedo at each time step consists of four components: direct and diffuse albedos for the VIS and NIR bands. In the model, each atmospheric grid cell over land is subdivided into up to five land cover types: glacier, lake, wetland, urban, and vegetation, which includes 1−4 of the 17 plant functional types (PFTs; including bare ground as one of the types).

CLM2 separately computes albedos for soil, snow, and vegetation, and then takes the total albedo of a grid box (α) as an average of these albedos weighted by the representative area fractions:

$$\alpha \ = \ \alpha_s f_s + \alpha_{sn} f_{sn} + \alpha_v f_v \quad , \qquad (1)$$

where α refers to albedo, f refers to fraction, and the subscripts s, sn, and v stand for bare soil (and glacier, lake, and wetland, if their area fractions are greater than zero), snow, and vegetation, respectively. The snow albedo is a function of grain size, soot and SZA. The soil albedo is a function of soil color and soil moisture but independent of SZA. The vegetation albedo in CLM2 is computed based on the two-stream approximation.

b. MODIS data

The global 1-km MODIS BRDF and albedo data (Schaaf et al. 2002) were derived by coupling all available cloud-free, atmospherically-corrected, spectral surface reflectance observations over a 16-day period with a semiempirical, kernel-driven BRDF model. MODIS data employed the Ross-Li BRDF model with three parameters and kernels. The three parameters are an isotropic parameter (f_{iso}) (describing the nadir bidirectional reflectance at nadir illumination), a radiative transfer or volumetric scattering parameter (f_{vol}), and a surface scattering or geometric optics parameter (f_{geo}).

Black-sky albedo (α_{bs}) is defined as the albedo in the absence of a diffuse component, and is a function of solar zenith angle. White-sky albedo (α_{ws}) is defined as the albedo in the absence of a direct component, and is independent of solar zenith angle. These two extremes can be combined as a function of the diffuse skylight fraction (S) for an actual albedo:

$$\alpha(\theta,\lambda) \ = \ (1-S)\alpha_{bs}(\theta,\lambda) + S\alpha_{ws}(\lambda) \quad . \qquad (2)$$

The SZA dependence of albedo can be adequately approximated by polynomials. The black-sky albedo is then

$$\alpha_{bs}(\theta,\lambda) \ = \ f_{iso}(\lambda) + f_{vol}(\lambda)h_{vol}(\theta) + f_{geo}(\lambda)h_{geo}(\theta) \quad , \qquad (3)$$

where θ is the SZA, and h is a known polynominal of θ.

The white-sky albedo is the integration the black-sky albedo over all SZAs:

$$\alpha_{ws}(\theta,\lambda) \ = \ f_{iso}(\lambda) + 0.189184 f_{vol}(\lambda) - 1.377622 f_{geo}(\lambda) \quad . \qquad (4)$$

Equations (3) and (4) are used to obtain the black-sky and white-sky albedos for each wavelength band. Finally, these results are converted to the visible (0.3−0.7 μm), near-infrared (0.7−5.0 μm), and shortwave (0.3−5.0 μm) broad band albedos using the empirical spectral-to-broad band conversion coefficients.

3. Evaluation of CCSM2 monthly averaged albedo

The standard output from most global climate models includes monthly averaged reflected and incoming solar radiation fluxes at surface, and their ratio is defined as the monthly averaged albedo. This would be consistent with the MODIS albedo computed using Eq. (2) weighted by the incoming solar fluxes. However, diffuse skylight fraction (S) is not readily available, and Eq. (2) can not be directly used. Since the white-sky albedo represents the integration of the black-sky albedo over all SZAs, it should be close to the model albedo.

Figure 1 shows that the overall spatial pattern of model albedo is consistent with that of the MODIS data. The CCSM2 albedo is lower by 0.05-0.2 than the MODIS albedo over deserts in North Africa and the Middle East. The model albedo is also higher by more than 0.05 over parts of the South America, southern Africa, and Australia. Over Northern Hemisphere high latitudes, the model albedo in July is also higher by more than 0.05, because there are too many snow-covered regions still left in the model.

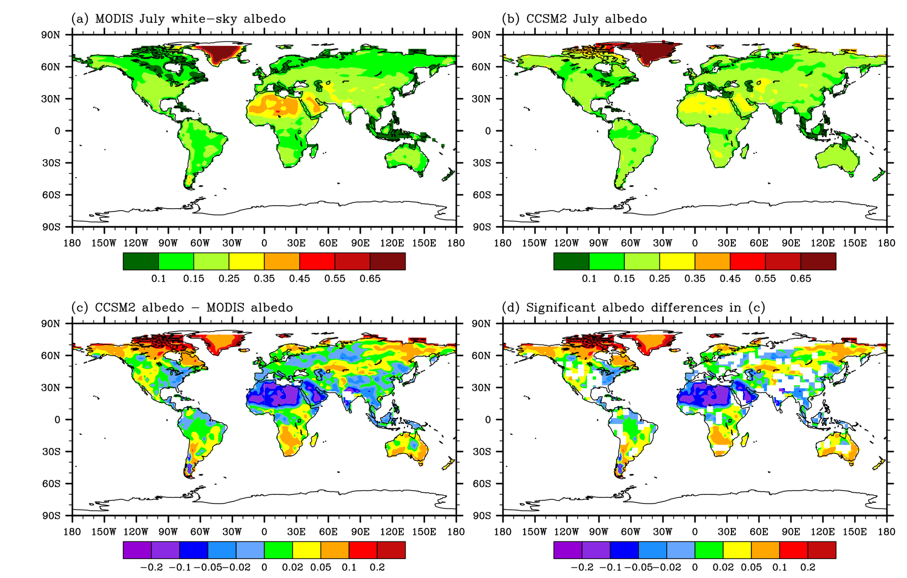

Figure 1: The global distribution of land surface albedo in July. (a) MODIS white-sky albedo (α_{ws}) in 2001, (b) CCSM2 monthly albedo averaged over 10 yr, (c) CCSM2 albedo − MODIS α_{ws}, and (d) significant (at 95% using student t-test) albedo differences in (c).

In the completely snow-covered nonforested regions, this difference may be partially due to an error in the coefficients used to convert narrowband albedos to broadband albedos over snow-covered regions. In this study, the focus is on snow-free areas.

The "MODIS average albedo" is introduced to decompose the difference field shown in Fig. 1c into two parts. MODIS average albedo refers to the albedo computed using the MODIS BRDF and albedo data that is fully consistent with the model albedo. The first part represents the deviation of CCSM2 albedo from MODIS average albedo and is due to model deficiency in the albedo parameterization. The second part reflects the inherent difference between albedo computed using the CCSM monthly averaging method and MODIS white-sky albedo. For comparison with model monthly average albedos, we need to average MODIS albedos over SZA.

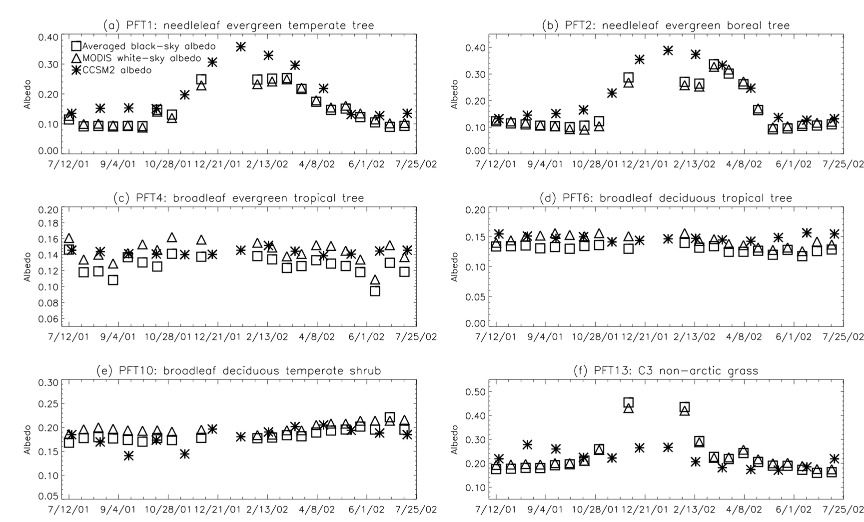

Figure 2: The seasonal variation of the 16-day MODIS white-sky albedo, CCSM2 monthly averaged albedo, and 16-day averaged MODIS black-sky albedo over six grid cells with different dominant PFTs. (a) PFT1, (b) PFT2, (c) PFT4, (d) PFT6, (e) PFT10, and (f) PFT13 (see Table 2 for the location of model grid cells).

Figure 2 shows the seasonal variation of the CCSM2 albedo, MODIS average black-sky albedo, and MODIS white-sky albedo over six model grid cells with different dominant PFTs (see Table 1). For needleleaf evergreen trees in Fig. 3a, the CCSM2 albedo agrees with the MODIS data well in June and July, but is slightly larger than the MODIS data in August and September. This indicates that results in a particular month are not necessarily indicative of results in other months. For needleleaf evergreen trees in Figs. 2a and 2b, the model albedo is much higher than the MODIS data in winter months. For broadleaf evergreen trees (Fig. 2c), model and MODIS albedos agree with each other very well. These values are also consistent with in situ measurements. The abrupt drop of MODIS albedo in early June 2002 and the larger seasonal variation of MODIS albedo than model albedo are related to the consistent cloud cover over this area. For broadleaf deciduous tropical trees (Fig. 2d), the CCSM2 albedo also agrees with MODIS data well. For broadleaf deciduous temperate shrub (Fig. 2e), the CCSM2 albedo is lower than the MODIS albedo from June to November. The relative large model versus MODIS albedo differences in September and November may be caused by the difference between the actual precipitation during these periods of the MODIS data and the 10-yr averaged model precipitation. For C3 nonarctic grass (Fig. 2f), the CCSM2 albedo is slightly larger than the MODIS value in August and September, but it is smaller in other months. Because of a lack of snow at this location in the model, the CCSM2 albedo is much smaller than the MODIS value in December and January.

4. Evaluation of the SZA dependence of model albedo

Hourly output of the four components of surface albedo was not saved in CCSM2 simulations. Therefore, to obtain this output, additional CAM2/CLM2 simulations are completed. We evaluate the SZA dependence of the model albedo over 11 grid cells with different dominant PFTs and over different regions (Table 1). We only choose the grid cells without fractional covers for glacier, urban, wetland, and lake. Hourly output of

Table 1: Location of 11 model grid cells with different dominant plant functional types (PFTs) along with their fractional area coverages. PFTs 1, 2, and 4, 6, 10, and 13 are used in Fig. 2, and PFT3 2 and 13 in Fig. 3. All PFTs are used in Fig. 4.

PFT	Area (%)	Center Lat/Lon	Geographic Region
1	53	(51.6°N, 120.9°W)	Canada
2	61	(57.2°N, 120.9°W)	Canada
3	57	(62.8°N, 115.3°E)	Siberia
4	79	(4.2°S, 73.1°W)	Amazon
6	44	(12.6°S, 53.4°W)	Brazil
7	60	(37.6°N, 81.6°W)	United States
9	43	(40.5°N, 8.4°E)	Italy
10	100	(20.9°S, 123.8°E)	Australia
11	91	(65.6°N, 90.0°E)	Siberia
12	82	(57.2°N, 132.2°E)	Russia
13	98	(46.0°N, 115.3°E)	Mongolia

the four components of CAM2/CLM2 albedo for a 16-day period (12−27 July 2001) are used. The comparison of SZA dependence between model and MODIS are shown in Fig. 3 for PFT 2 (needleleaf evergreen boreal tree) and PFT 13 (C3 nonarctic grass). For θ larger than 70°, the input surface reflectances for retrieval are usually poor, and the polynomial representation in Eq. (3) is not as accurate either. Therefore, our discussions are limited to SZA less than 70°.

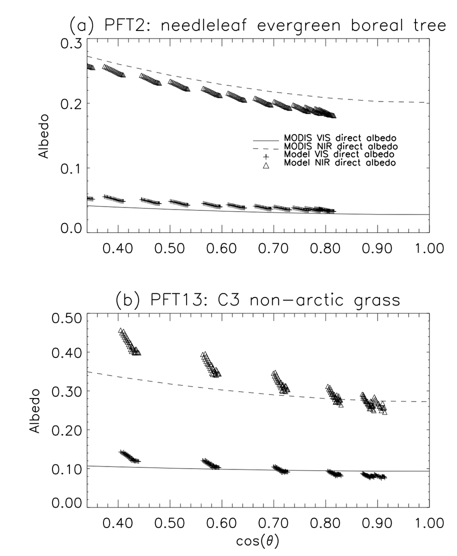

Figure 3: Comparison of the SZA dependence between the CAM2/CLM2 hourly direct albedo and MODIS direct albedo for (a) PFT 2, and (b) PFT 13 (see Table 2 for the location of the model grid cells). Only results for θ < 70° shown. Model results are based on the CAM2/CLM2 hourly output for a 16-day period (12−27 Jul 2001). The MODIS direct albedo data obtained from Eq. (3) using the MODIS BRDF parameters for the same period.

Figure 3 shows that both model and MODIS direct albedos decrease monotonically with cosθ. However, the model direct albedo increases too fast with the increase of SZA (or with the decrease of cosθ). This pattern is also evident for most PFTs in Table 1. The model overestimates VIS direct albedo and underestimates NIR direct albedo for PFT 2 (Fig. 3a). The model (VIS and NIR) direct albedo is closer to the MODIS albedo at local noon (i.e., at a higher cosθ) than in the morning or afternoon for PFT 13 (Fig. 3b).

Figure 4 shows the 10th, 25th, 50th, 75th, and 90th percentiles of the differences between the model and MODIS direct albedos for the 11 grid cells in Table 1. Figure 4a shows that the difference between the 90th and 10th percentiles for the VIS band is less than 0.02 for all grid cells except for PFT 13, while Fig. 4b demonstrates that the corresponding difference for the NIR band is less than 0.02 for only six cells (PFTs 2-4, 7, 10, and 11), and is as large as 0.1 for PFT 13 and 0.07 for PFT 12.

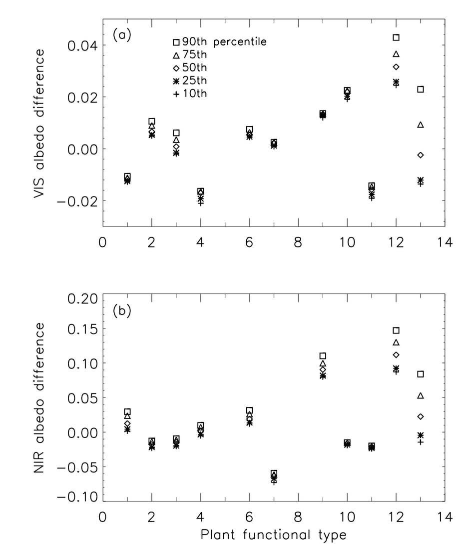

Figure 4: The 10th, 25th, 50th, 75th, and 90th percentiles of the differences between the CAM2/CLM2 hourly direct albedo and MODIS direct albedo (a) in the VIS band, and (b) in the NIR band for the 11 grid cells with different PFTs.

5. The SZA dependence of desert and vegetation albedos

Most land surface models assume that the bare soil albedo is a function of soil color and moisture but independent of SZA. However, analyses of the MODIS BRDF and albedo data indicate that bare soil albedo does vary with SZA. This is confirmed using in-situ data. The vegetation albdo is calculated based on two-stream method, which does not consider the 3-D structure of the canopy. The global 0.05° MODIS BRDF/albedo data (version 4) are used in this study. Only the data derived primarily from full inversion under snow-free condition are used. We analyze all of the BRDF data available from 2000 to 2004. Based on MODIS Land Cover Type (MOD12) and fractional vegetation cover dataset derived from MODIS NDVI data, we have identified thirty 0.05° pixels representing each of the major deserts of the world with zero fractional vegetation cover to examine the SZA dependence of desert albedo. Similarly, we do the same work for all IGBP vegetation types.

At each pixel, the black-sky albedo and its SZA dependence do not change much during all 16-day periods. For each location, there is a median albedo among all 16-day periods at each SZA, so a curve can be obtained from median albedos over all SZAs. Figure 5a,b shows these median SZA dependence curves of black-sky albedo over all thirty pixels. The significant geographic variation of desert albedo is consistent with previous studies (Tsvetsinskaya et al. 2002). To see the SZA dependence more clearly, we normalize each curve in Fig. 5a,b by its value at 60 ° SZA, and results are shown in Fig. 5c,d. While the albedo increases with SZA over each pixel, its variation with SZA is quantitatively different over different pixels.

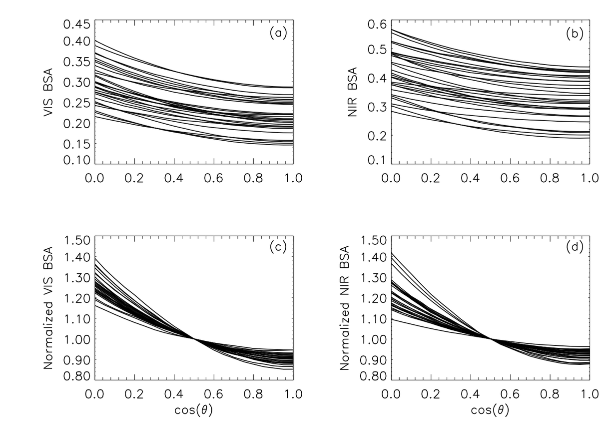

Figure 5: The mdian curves of the MODIS black-sky albedos in (a) VIS and (b) NIR band versus the cosine of SZA at 30 desert locations. The normalized curves with respect to their albedo values at 60 ° SZA are shown in (c) VIS and (d) NIR band.

To adequately describe the SZA dependence of bare soil albedo as given in Fig. 5, we rewrite the MODIS BRDF/albedo algorithm:

$$\alpha(\theta) \ = \ \alpha_r[1 + C_1[g_1(\theta) - g_1(60°)] + C_2[g_2(\theta) - g_2(60°)]] \quad . \qquad (5)$$

where α is the black-sky albedo, θ is the SZA. In this new formulation, only the albedo at 60° SZA (α_r) depends on season and location. The functions g1 and g2 are from the MODIS algorithm. The parameters B1 and B2 are the ratios of the volumetric and geometric parameters in the MODIS algorithm over α_r, respectively. Fig. 6a-d shows these parameters in the VIS and NIR bands for thirty pixels as a function of α_r. Based on this figure, we obtain B1=0.036 and B2=0.063.

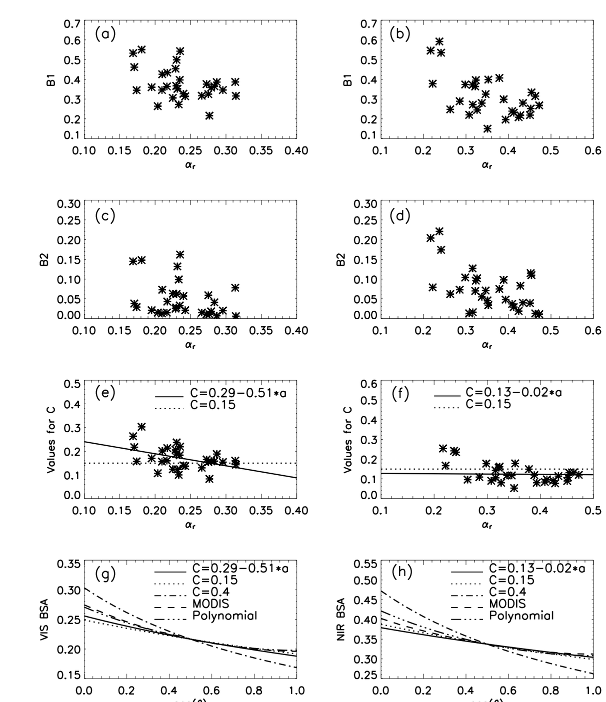

Figure 6: The median B1 vs. MODIS black-sky albedo at 60° (α_r) for 30 desert pixels in (a) VIS and (b) NIR band. The median B2 vs. α_r in (c) VIS band and (d) NIR band. The values for C vs. α_r in (e) VIS band and (f) NIR band (solid line: the best-fit linear function; dotted line: the average C value of VIS and NIR bands). (g) The SZA dependence at a pixel (19.975°N, 43.325°E) using the MODIS data directly and computed using (5) and (6) with different C (the best-fit linear function or fixed values) in the VIS band; (h) Same as (g) except in the NIR band.

We have also tested the simple formulation (Briegleb et al. 1986):

$$\alpha(\theta) \ = \ \alpha_r[(1+C)/(1+2C\cos(\theta))] \quad . \qquad (6)$$

where the empirical parameter C was taken as 0.4 for arable grass and desert, and 0.4 for all other types. Equation (6) and the above C values have also been used in the remote sensing retrieval of land surface solar fluxes and in some land-atmosphere coupled models.

A more apprporiate C value can be determined by the weighted least square method.The weighting factor of cos(θ) is the same as that used for computing the white-sky albedo. This is chosen also because MODIS data are more reliable at SZA less than 70° and because the albedo is more important at a smaller SZA when solar flux itself is large. The values for C over all thirty pixels are plotted as a function of α_r in Fig. 6e,f. Their mean values of VIS and NIR bands are 0.17 and 0.13, respectively, and their average of 0.15 is used for both bands to be consistent with Briegleb et al. (1986).

To compare the performance of (5) and (6), we compute the average standard deviation from MODIS data. The values are 0.0061, 0.0081, and 0.0072 using the two-parameter model, one-parameter with constant C as well as the best-fit linear equations, respectively. This shows the two-parameter model is a lottle better than the one-parameter model. If the white-sky albedo is used (i.e., without considering the SZA dependence), the standard deviation would be 0.0195 and is much bigger than those using (5) or (6). This indicates the importance of the SZA dependence. Figure 6g,h evaluates the SZA dependence over a pixel (19.975°N, 43.325°E) using (5) and (6) with different C values. The simulated SZA dependence using two-parameter model, one-parameter model with the best-fit linear equation or the C value fixed at 0.15 are consistent with the MODIS data for SZA less than 60°. In contrast, the alnedo computed with C=0.4 increases with SZA much faster than indicated by the MODIS data.

Similarly, we have done the same work on all IGBP vegetation types. As an example, Figure 7 evaluates the SZA dependence over a pixel (35.325°N, 111.625°W) using (5) and (6) with different C values. The simulated SZA dependence using the two-parameter, one-parameter model with the best-fit linear equation or C=0.34 are consistent with the MODIS data for SZA less than 60°. However, the albedo computed with C=0.1 underestimates the SZA dependence relative to the MODIS data. The standard deviations from MODIS data using two-parameter as well as one-parameter model with C=0.34 or the best-fit linear equation are much smaller than that using MODIS white-sky albedo. However, the empirical parameters B1, B2, and C depend on plant functional type .

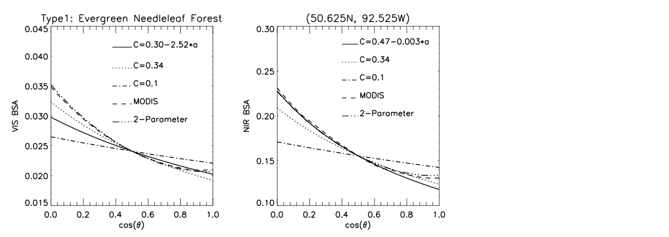

Figure 7: The SZA dependence at a pixel (35.325°N, 111.625°W) using the MODIS data directly and computed using (5) and (6) with different C in the VIS and NIR band.

Based on these analysis, we recommend the use of the polynomial Eq. (5) or Eq. (6) with C=0.15 over bare soil with in land modeling and remote sensing retrieval of land surface solar fluxes. Different C value will be used for different vegetation type. Then the white-sky albedo can be obtained analytically by integrating Eqs. (5) and (6) over al SZA's.

6. Conclusions

The recent availability of the MODIS BRDF/albedo data makes it possible to evaluate and improve the treatment of albedos in global models. The NCAR CCSM2 significantly underestimates albedo throughout the year over deserts (e.g., the Sahara Desert). The model versus MODIS albedo difference is larger than 0.05 over some other regions, particularly over semiarid regions (e.g., Australia). We have also selected 11 grid cells with different dominant plant functional types to evaluate the SZA dependence of the CAM2/CLM2 albedo. Both MODIS and model direct albedos generally increase with the increase of SZA. However, model direct albedo usually increases faster than MODIS data over most of these grid cells. These albedo differences between CCSM2 (or CAM2/CLM2) and MODIS are related to the deficiencies in the model simulation of snow cover and soil moisture and in the model's specification of LAI and SAI. Over regions with consistent cloud cover, the albedo difference between the model and MODIS data may also be partially caused by the uncertainty of the MODIS data based on the magnitude (rather than full) inversion. The albedo biases are also partially caused by the deficiency of the two-stream method used to compute albedo in the model. The preceding analyses combined with the MODIS BRDF and albedo data provide a starting point towards developing a BRDF-based treatment of radiative transfer through canopy for land surface models that can realistically simulate the mean albedo and the SZA dependence of albedo.

Our analysis of the MODIS and insitu data indicate that the bare soil albedo depends on the SZA, and this dependence can be adequately represented by Eq. (5) with B1=0.346 and B2=0.063 as well as Eq. (6) with C=0.15. These dependences need to be considered in land surface modeling. Further work is also needed to evaluate the impact of these formulations on the remote sensing retrieval of land surface solar fluxes.

Acknowledgments. This work was supported by NASA through its EOS IDS Program (429-81-22; 428-81-22). The first three authors were also supported by NOAA under grant NA06GP0569 and by NOAA under grant NA03NES4400013.